(5) 372 950

(4) $4.60

THE BUCKLING OF THIN WALLED CIRCULAR CYLINDRICAL SHELLS UNDER COMBINED AXIAL COMPRESSION AND BENDING

(7) NH

(8) NH

(9) NH

(10)

~~Thesis by~~
Floyd R. Stuart
Captain, United States Air Force

(11) 1963

(12) 39 p.

(13) NH

(14) NH

(15-19) NH

(20) 11.

(21) NH

THE BUCKLING OF THIN WALLED CIRCULAR CYLINDRICAL SHELLS UNDER COMBINED AXIAL COMPRESSION AND BENDING

Thesis by

Floyd R. Stuart

Captain, United States Air Force

In Partial Fulfillment of the Requirements

for the Degree of

Aeronautical Engineer

California Institute of Technology

Pasadena, California

1963

ABSTRACT

An experimental investigation of the interaction of combined axial compression and bending stresses on the buckling of cylindrical shells of similar geometry was carried out.

The shells tested were manufactured by a copper electroforming process. This method of fabrication produced thin shells to close geometric tolerances without the usual seams.

A total of 16 buckling tests were conducted. The resulting experimental interaction curve indicates that the critical buckling stress increases with increased bending moments.

ACKNOWLEDGMENTS

It is the author's desire to express his sincere gratitude to those who helped, through their guidance, suggestions and genuine interest to make this study possible. Especially:

To Dr. E. E. Sechler, whose interest and guidance made this problem tractable, and, therefore, possible.

To Dr. C. D. Babcock, for his many hours of assistance and helpful suggestions.

To Mr. L. V. Schmidt, for his assistance in programming the reduction of data.

To Mr. A. Abu-Shumays, for his help with test specimen production.

To Miss Helen Burrus, for preparation of the final form of this thesis and

To my wife, for her unfailing confidence.

LIST OF TABLES

LIST OF FIGURES

LIST OF FIGURES (cont'd)

LIST OF SYMBOLS

A_o	Constant coefficient resulting from Fourier analysis of buckling data
B_n	Harmonic coefficients resulting from Fourier analysis of buckling data
E	Young's Modulus
K_b	Strain gage factor, $\left[\frac{\text{in-lbs}}{\text{mv}}\right]$, bending moment
K_c	Strain gage factor, $\left[\frac{\text{lbs}}{\text{mv}}\right]$, axial compression
L	Cylinder length
M	Applied bending moment $\left[B_1 K_b\right]$
R	Cylinder Radius
t	Cylinder thickness
σ_c	Applied axial stress $\left[\frac{A_o K_c}{2\pi R t}\right]$
$\bar{\sigma}_c$	Theoretical buckling stress for long cylinder under axial compression $\left[\frac{E}{\sqrt{3(1-\nu^2)}} \quad \frac{t}{R}\right]$
C_σ	Non-dimensional axial compression buckling coefficient $\left[\frac{\sigma_c R}{Et}\right]$
$C_{\bar{\sigma}}$	Theoretical non-dimensional axial compression buckling coefficient $\left[\frac{\bar{\sigma}_c R}{Et}\right]$
C_b	Non-dimensional bending moment buckling coefficient $\left[\frac{M}{\pi E t^2 R}\right]$
ν	Poisson's Ratio
θ	Angle denoting circumferential position on test specimen
φ_n	Phase angle resulting from Fourier analysis of buckling data

I. INTRODUCTION

With the advent of missiles and spacecraft the question of thin shell stability has taken on new importance. The necessity for weight reduction has placed ever increasing demands upon the designer. No longer can he apply large safety factors to his design, yet it is not economically sound to expose a costly and sophisticated payload to possible destruction due to failure of one of its auxiliary components.

It is important then that a better understanding be gained of the reaction of shells and shell-like structures to complex loading.

The combination of axial compression and bending arises naturally from the flight of a missile or spacecraft. It is an area that has not been extensively investigated. The author is aware of only two experimental evaluations of the interaction curve for this particular combination (Refs. 1 and 2).

Until recently the theoretical value of critical bending stress was accepted as that presented by Flügge namely $1.3\,\bar{\sigma}_c$ (Ref. 3). It has been shown (Ref. 4) that Flügge's calculation was quite restricted and a more general investigation has lead to the conclusion that the maximum stress to cause buckling under bending is identical to the value for compression.

Experimental investigations of shell stability have been, and for the most part are, quite discouraging. The correspondence with theory ranges from 15 to 60 $^{o}/o$ with considerable scatter (Ref. 5).

There are indications, however, that much can be done to improve this situation by careful fabrication of test specimens and control of experiments. Babcock (Ref. 6) has demonstrated that a substantial increase in buckling load can be obtained through employment of the above techniques.

This study has been undertaken to determine experimentally the interaction curve between axial compression and bending. An attempt has been made to use as nearly perfect specimens as possible and to monitor and report all observable deviations from the "perfect" assumptions.

In order to eliminate, as far as possible, the various effects of initial imperfections and seams, the test shells were carefully manufactured and tested for imperfections prior to actual buckling tests.

A controlled end displacement testing machine, designed and used previously by Babcock (Ref. 6), for axial compression tests, was used to apply the combined loading.

II. EXPERIMENT

1. Shell Manufacture

The electroforming process previously reported in reference 6 was again used. Briefly the method consists of plating a copper shell on an accurately machined and silver painted wax form. After plating, the shell is removed by melting away the wax. The test specimens were plated on mandrels of 8.000" diameter and were cut to lengths of approximately 10 inches.

The wax form was cast over a hollow steel mandrel 13 inches long and 7 inches in diameter which was water cooled to harden the wax. After cooling, the mandrel was machined and spray painted with silver paint thinned with toluene. Figure 1 shows a steel mandrel and completed wax form.

The shell was then plated in a Cupric Fluoroborate, $Cu(BF_4)_2$, bath using a 15 inch diameter copper anode bagged in Dynel fabric. During plating the shell was rotated and the bath agitated with forced air. D.C. voltage was maintained at approximately 4 volts and current at 130 amperes.

Plating times of one hour and thirty minutes were used, after which the shell was removed from the bath, washed in water and cut to the desired length. The wax was then melted to remove the shell. Final cleaning was done in benzene to remove the residual wax and silver paint.

Two improvements were made in the above process to provide more uniform properties and better control. It was found that the

plating bath became heated approximately 10 to 15°C per hour during plating. This heating caused the wax mandrels to enlarge somewhat resulting in unintentional variation of shell radius and some internal stresses. Temperature variation was practically eliminated through use of polyethelene cooling coils, carrying tap water, which were submerged in the bath. This resulted in reducing temperature change to approximately 1 to 2°C per hour.

Secondly, continuous filtration of the plating bath was introduced. A Sethco, model LPM-20CC, continuous filter and pump was selected because of its capacity and ability to handle the corrosive solution. Noticable reduction in surface roughness was obtained through this addition.

2. Thickness Measurements

Shell thickness was obtained by accurately weighing the cleaned shell and dividing this by the surface area and density. A density of 8.9 grams per cubic centimeter was used for these and all thickness calculations.

Thickness variation throughout the shell was determined by computing the thickness of small circular discs which were cut from various locations on the shell after buckling tests were completed. Table II gives the results of these tests and indicates that variations were held to $\pm$ 3 °/o.

3. Material Properties

a. Poisson's ratio was taken as 0.3 for all calculations in this report.

b. Young's modulus

The value of Young's modulus used for calculations in this report was an average of several tests conducted on specimens from each shell. These tests were all conducted by the author. Each specimen was tested in uniaxial tension in the same Instron testing machine. The specimens were soldered into brass plates that were clamped into the jaws of the testing machine. Head displacement was used to measure strain and load was obtained from the machine load cell. The results of these tests were quite discouraging. There was considerable scatter among specimens from the same shell and also among average values for the shells. For this reason the value of Young's modulus used was the average value obtained for the individual shell. Table III presents the results of these tests and the value used for each shell. A typical stress strain curve for plated copper is given in Figure 8.

The reason for such wide scatter in the results of these tests is not known. A calibration of the Instron machine indicated that it was deflecting under load. A correction factor for displacement as a function of load was obtained by clamping a steel bar, large compared to the test specimens, in the jaws which had been moved together. This method is recommended by the manufacturer. A correction factor of 1.66×10^{-3} in/50 lbs. was obtained and all data in Table III has been corrected using this factor.

The variation in E from shell to shell becomes more reasonable when the results of Read and Graham (Ref. 9) are considered. They obtained values of E for electrodeposited copper ranging from 14 to 17 x 10^6 psi. Their conclusions were that the value of E for electrodeposited copper depended entirely upon the granular structure of the material, with small grains giving higher E. The granular structure of the shells for this work was not determined.

4. Initial Imperfection Measurements

After the shell was partially mounted in the testing machine measurements were taken to determine the deviation of the cylinder generators from a straight line. These measurements were taken with a pickup that could be positioned to any desired place on the shell. A set of ways was attached lengthwise along the cylinder and the pickup was moved along the ways. The pickup was calibrated prior to each test and data, obtained in voltages, was reduced to deflections by the calibration curve.

The ways were moved around the circumference and readings were taken every 40 degrees. The vertical stations were taken at 1/2 inch intervals along the length. Figures 18 to 20 show typical plots of these test results.

The pickup used was an iron core coil reluctance type which changes impedance to a given signal when its electromagnetic field is disturbed by eddy currents generated in an external conducting surface. The pickup output was approximately 25 volts per inch with a working range of about 0.200 inches. The impressed signal was

100,000 cps. Noise level and drift were such that deflections of 10^{-4} inches could be accurately determined.

5. Test Procedure

The completed shell was first mounted in a brass end ring with a low temperature alloy, Cerrobend. After the Cerrobend hardened, the other end of the shell was mounted in the load ring of the testing machine again using Cerrobend. With the shell so mounted, initial imperfection data were taken (Figure 2).

The testing machine was then rotated to the testing position and the free end of the shell rigidly attached to the machine end plate with Devcon Plastic Steel. Figure 3 shows testing machine and shell in testing position. Devcon was used since it is quite rigid when hardened and would fill in the areas where the end plate and end ring did not match perfectly. While the Devcon was hardening the machine was pre-loaded with springs. The springs were not used during testing.

Although the testing machine was originally designed for axial compression loading it was possible to apply a bending moment by varying the displacement of the end plates through nonuniform adjustment of the three adjusting screws. Close control of end plate movement was available since a single revolution of the adjusting screw corresponded to 0.025 inch displacement.

The total applied load and distribution was determined from data obtained from a load ring, (Figure 4). This was a brass cylinder 8.000 inches in diameter, 2.50 inches long and 0.0107 inches thick. Twenty-four strain gages were mounted around the inside and outside circumference at equally spaced stations, inside and outside gages

being directly opposite. The load ring gages were connected in series with 24 additional gages mounted on a brass plate for temperature compensation.

Each load ring gage was connected through a Wheatstone bridge, which provided zero balance, to a Leeds and Northrup amplifier where bridge output was amplified by a factor of five. Amplifier output was then connected to a Leeds and Northrup voltage meter from which data was recorded.

The load ring was calibrated at the completion of these tests to determine the load factor, K_c, versus strain gage reading for axial compression. The results of this calibration are given in Figure 6.

The actual testing was carried out in the following manner. After the shell was properly mounted the desired difference in strain gage reading was adjusted at 180° positions on the shell. This could be accomplished with considerable accuracy as interaction around the circumference of the shell due to adjustment of a single load screw was minimal. Once the desired moment was applied all three screws were adjusted simultaneously thereby applying axial compression. Data was taken at approximately 50 $^{\circ}/o$ expected buckling load and at small increments thereafter. Throughout the axial compression phase individual adjustments were made to maintain the desired applied moments. The axial compression load was increased until buckling occurred and the highest strain gage reading observed at buckling was recorded.

Two additional tests were accomplished to determine the load factor, K_b, for applied bending load and to check K_c and K_b under combined loading. A simple beam was attached to the top end plate of a shell and dead weight loaded in increasing increments. As loading was increased strain gage readings were recorded. This data was reduced by Fourier analysis and a value for K_b of 610 in lb/millivolt was obtained. The results are given in Figure 6. The test set up is shown in Figure 5.

6. Test Results

As previously stated it was the intention of this investigation to determine an interaction curve for axial compression and bending of circular cylindrical shells. No initial imperfections were intended nor was it intended to investigate the R/t parameter.

A total of 16 shells were tested. Table I gives a description of the specimens, and Table V the results of the tests. It was attempted to completely cover the range of interaction between these two loadings. After the first nine tests were completed and the data reduced it was apparent that the desired coverage had been obtained and the remaining seven tests were conducted to determine scatter. As Figure 7 shows the interaction curve can be well approximated by a straight line.

Buckling occurred in all tests with complete failure and subsequent load reduction. There were no cases of local buckling occurring prior to failure.

The post-buckle state was the familiar diamond shaped pattern which occurred in several rows around the circumference for most

cases. The shells tested under high moments, buckled only on the compression side. There seemed to be no preferred end at which buckling occurred and pattern size was not noticably different at either end of the curve.

During the tests all twenty-four gages were monitored and recorded. Variation between inner and outer gages was quite small and in most cases less than 5 ^{o}/o of the total load.

The strain gage readings used to calculate buckling loads were averages of inside and outside gages of the load ring. As it was not possible to monitor all gages simultaneously during actual loading, the intended high compression gage was selected as the gage to be monitored. Since buckling usually occurred during loading it was necessary to adjust the remaining gages to the level of the monitored high compression gage. This adjustment was accomplished by an averaging process over previous increments prior to buckling.

After all gages were adjusted to the buckling value and averaged, the data was reduced by Fourier analysis carried out on an IBM 7090 digital computer. The method employed was that described in reference 7, and the data presented in the form

$$\text{strain gage reading} = A_o + \sum_{n=1}^{6} B_n \cos(\theta - \varphi_n)$$

The constant term and first harmonic coefficients were used to calculate applied loads and stresses. Table IV gives the complete results of this analysis, and Figures 8 through 16 show the correspondence between actual strain gage readings and the Fourier representation used to calculate buckling stresses.

7. Experimental Difficulties

As previously mentioned the testing machine used was originally designed for axial compression tests only, and when it was attempted to apply a pure bending moment it became apparent that the end plates of the machine were also bending. Two attempts were made to improve load distribution by stiffening the end plate and providing additional adjustments around the shell circumference. A one inch steel plate was attached to the end plate of the machine upon which three additional load screws could be brought to bear. It was thought that this additional strength and latitude of loading would improve the applied moment. This did not occur however, as the steel plate was actually too rigid and would not transmit loads satisfactorily. The second attempt was essentially the same except this time a 0.75 inch lucite plate was used. This plate did transmit loads but it also introduced local bending in the shell and was therefore unsatisfactory. It was then decided to accept the load distribution available and continue with the investigation realizing that the applied moment was not quite pure.

It should also be mentioned that obtaining data at the high bending moment end of the curve was difficult. In several tests the moments required produced large tensile stresses on one side of the shell. It was noted that in some cases these stresses would relax significantly, on the order of 5 $^{o}/o$ of the total load, and the test had to be abandoned. This relaxation is contributed to the mounting process employed. Apparently the Cerrobend bond was not strong

enough to hold under these extreme conditions. This problem was avoided by selecting the thinnest specimens for this portion of the tests.

8. Conclusions

The interaction curve, Figure 7, was obtained by normalizing the experimentally obtained buckling coefficients with the theoretical value for axial compression which is assumed to be the critical value for both axial compression and bending, reference 4. The empirical curve is a least-square fit to the data points.

The agreement with theory is quite good at the bending end of the curve, and decreases as the ratio of axial compression to bending increases. This would seem to indicate that there is something peculiar to bending that makes the shell less susceptible to such phenomena as initial imperfections or the Poisson expansion of the cylinder boundaries.

Experimental data, taken just after buckling before the loading was changed, indicates that a sharp decrease in moment accompanies failure. This would appear to indicate that initial imperfections should be as critical for bending as axial compression. The Poisson expansion of the cylinder boundaries may be an explanation of the disagreement, if this effect can be shown to be a linear one that disappears under pure bending. It therefore seems desirable that a large deflection theory for pure bending be developed including the effects of initial imperfections and or Poisson expansion to determine just how significant these may be.

9. Recommendations for Future Research

The effects of Poisson expansion, initial imperfections and radius-thickness ratio should be investigated experimentally for the present load configuration. It has been demonstrated in reference 6 that initial imperfections of various dimensions can be achieved through the electroforming process. Tests using other load combinations should also be carried out.

The load ring has proven quite satisfactory for measuring axial compression and bending. This same approach might also be used to determine torsional loads through employment of strain gage rosettes.

A simple, accurate method of determining Young's modulus for thin specimens is needed. An adaptation of the method described in reference 9 could possibly be the answer.

An all purpose testing machine would be extremely valuable but very difficult to design. It is felt that the load distribution could have been better controlled if additional loading points were available. It seems that four points should be a minimum.

The process of measuring initial imperfections was quite tedious and yielded no information about deviations from circular shape. What is needed is a circumferential traversing mechanism that can be accurately positioned with reference to the shell center. Absolute measurements would be quite difficult to obtain to the required accuracy, however relative deviations among specimens might prove important.

REFERENCES

1. Bruhn, E. F.: Tests on Thin-walled Celluloid Cylinders to Determine the Interaction Curves under Combined Bending, Torsion, and Compression or Tension Loads. NACA TN 951, (January 1945).

2. Weingarten, V. I., Morgan, E. J.; and Seide, P.: Final Report on Development of Design Criteria for Elastic Stability of Thin Shell Structures. Space Technology Laboratories, Report No. STL/TR-60-0000-19425 (EM 10-26), (December 1960), pp. 127-132.

3. Flügge, W.: Die Stabilitaet der Kreiszylinderschale. Ingenuni-Archiv, Vol. 3, (1932), pp. 463-506.

4. Seide, P.; and Weingarten, V. I.: On the Buckling of Circular Cylindrical Shells under Pure Bending. Space Technology Laboratories, Report No. TR-59-0000-00688 (EM 4-11) (June 1959).

5. Fung, Y. C.; and Sechler, E. E.: Instability of Thin Elastic Shells. Reprinted from Structural Mechanics, Pergamon Press, Oxford, London, New York, Paris (1960), pp. 115-116.

6. Babcock, C. D., Jr.: The Buckling of Cylindrical Shells with an Initial Imperfection under Axial Compression Loading. Ph. D. Thesis, California Institute of Technology (1962).

7. von Kármán, T.; and Biot, M. A.: Mathematical Methods in Engineering, McGraw Hill Book Co., Inc., New Yor, (1940), pp. 336-338.

8. Scarborough, J. B.: Numerical Mathematical Analysis. Fifth Edition, The Johns Hopkins Press, Baltimore (1912).

9. Read, H. J., and Graham, A. H.: The Elastic Modulus and Internal Friction of Electrodeposited Copper. Journal of Electro Chemical Society, Vol. 108, No. 2, (1961).

TABLE I

DESCRIPTION OF TEST SPECIMENS

Shell	Length inches	Thickness inches x 10^3	R/t
S-1	9.97	4.78	838
S-2	9.98	4.69	855
S-3	10.03	4.97	805
S-4	9.97	4.78	838
S-5	9.98	4.68	855
S-6	10.00	4.91	815
S-7	10.00	4.60	870
S-8	9.97	4.78	836
S-9	9.97	4.85	825
S-10	9.97	4.76	824
S-11	9.97	4.31	925
S-12	9.97	5.02	797
S-13	9.97	5.48	730
S-14	9.97	5.04	795
S-15	9.97	5.12	783
S-16	9.97	3.97	1000

TABLE II

THICKNESS VARIATION OF SHELLS

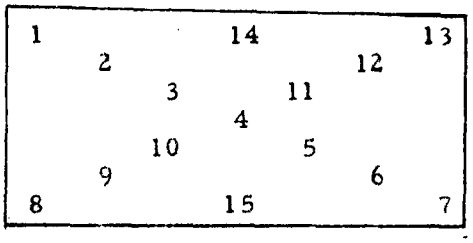

Numbers indicate position on shell at which thickness specimens were cut.

Thickness inches x 10^3

Position	Shell S-8	Shell S-11	Shell S-12
1	4.82	4.31	5.00
2	4.87	4.36	4.88
3	4.88	4.40	4.85
4	4.80	4.39	4.94
5	4.72	4.34	5.05
6	4.66	4.26	5.17
7	4.65	4.19	5.21
8	4.88	4.26	4.89
9	4.89	4.34	4.81
10	4.85	4.40	4.82
11	4.74	4.35	4.97
12	4.69	4.28	5.17
13	4.68	4.23	5.17
14	4.81	4.39	4.98
15	4.77	4.41	4.92
Average	4.78	4.33	4.99

TABLE III

YOUNG'S MODULUS TEST RESULTS

Shell	E psi x 10^{-6}	$\frac{E_{max} - E_{min}}{E_{ave}}$ %
S-1	15.3	9.2
S-2	16.7	2.0
S-3	15.1	12.0
S-4	15.0	6.6
S-5	15.3	4.6
S-6	15.7	5.2
S-7	14.9	8.0
S-8	16.0	5.0
S-9	16.8	7.2
S-10	15.9	9.4
S-11	16.0	7.6
S-12	16.5	2.4
S-13	15.8	9.4
S-14	15.6	11.6
S-15	15.8	5.0
S-16	14.9	9.4

TABLE IV

RESULTS OF FOURIER ANALYSIS*

Strain gage reading = $A_o + B_n \cos(\theta - \varphi_n)$; n = 1, 2 . . .

Shell	A_o	B_1	φ_1	B_2	φ_2	B_3	φ_3	B_4	φ_4	B_5	φ_5	B_6	φ_6
S-1	145.4	96.8	-24°	9.6	-26°	2.5	-66°	0.8	-81°	3.9	2°	0.4	0°
S-2	340.1	6.5	10°	8.9	31°	9.3	-86°	5.3	-31°	3.4	-69°	1.9	0°
S-3	264.4	63.5	-35°	10.9	58°	8.6	-80°	3.2	-45°	1.9	64°	0.2	0°
S-4	209.9	145.6	-25°	13.9	25°	4.0	75°	2.2	68°	2.2	-88°	2.1	0°
S-5	282.7	44.4	-19°	11.2	-59°	7.5	-37°	3.4	40°	1.5	-22°	2.9	0°
S-6	111.7	204	-30°	16.8	-77°	4.4	24°	2.4	-79°	1.8	48°	0.5	0°
S-7	108.1	249.7	-32°	19.6	-67°	3.8	23°	2.4	-37°	3.0	-19°	0.7	0°
S-8	268.3	118.8	-34°	18.6	51°	9.1	55°	3.6	-45°	0.9	-46°	1.2	0°
S-9	213.0	150.1	-29°	9.3	-67°	11.5	- 4°	14.2	73°	5.4	-72°	5.3	0°
S-10	165.0	232.2	-33°	28.4	77°	6.1	69°	5.0	-31°	3.0	-82°	0.2	0°

* Tabulated values are strain gage readings in mv x 10^2 at buckling.

TABLE IV (cont'd)

RESULTS OF FOURIER ANALYSIS*

Strain gage reading = $A_o + B_n \cos(\theta - \varphi_n)$; n = 1, 2 . . .

Shell	A_o	B_1	φ_1	B_2	φ_2	B_3	φ_3	B_4	φ_4	B_5	φ_5	B_6	φ_6
S-11	51.6	307.3	-28°	29.9	-59°	4.1	-87°	15.3	82°	5.4	88°	1.6	0°
S-12	331.3	125.9	-17°	10.8	22°	16.2	18°	7.7	-69°	6.6	- 5°	0.2	0°
S-13	169.1	297.4	-35°	39.1	-88°	4.7	-75°	6.6	40°	7.9	-29°	1.3	0°
S-14	202.6	209.8	-25°	11.9	3°	6.6	72°	5.9	-76°	2.7	85°	2.5	0°
S-15	380.8	16.5	6°	10.5	-35°	9.4	-69°	2.8	- 4°	3.1	-25°	0.4	0°
S-16	25.7	263.0	-31°	10.0	-71°	4.4	59°	2.8	58°	1.9	54°	2.6	0°

* Tabulated values are strain gage readings in mv x 10^2 at buckling.

TABLE V

SUMMARY OF BUCKLING DATA

Shell	σ_b max (psi)	σ_c max (psi)	C_σ	C_b
S-1	2456	3332	.187	.134
S-2	168	7945	.417	.01
S-3	1551	5828	.319	.083
S-4	3695	4811	.274	.205
S-5	1150	6618	.38	.064
S-6	5040	2492	.133	.261
S-7	6586	2575	.154	.384
S-8	3015	6150	.33	.158
S-9	3755	4811	.243	.184
S-10	5920	3798	.206	.313
S-11	8650	1310	.078	.501
S-12	3042	7230	.367	.150
S-13	6586	3380	.160	.304
S-14	5052	4403	.23	.257
S-15	391	8148	.414	.019
S-16	8038	708	.049	.543

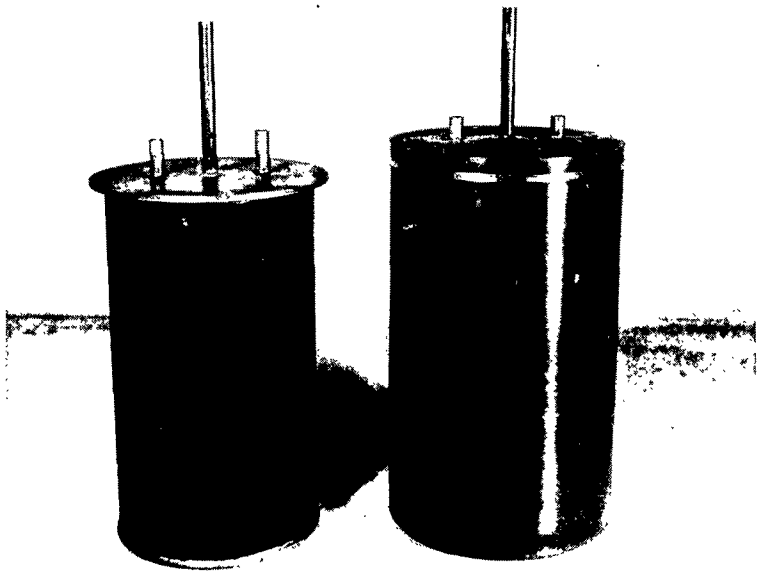

Fig. 1. Steel Mandrel and Completed Wax Form. Photograph courtesy of C. D. Babcock, Jr.

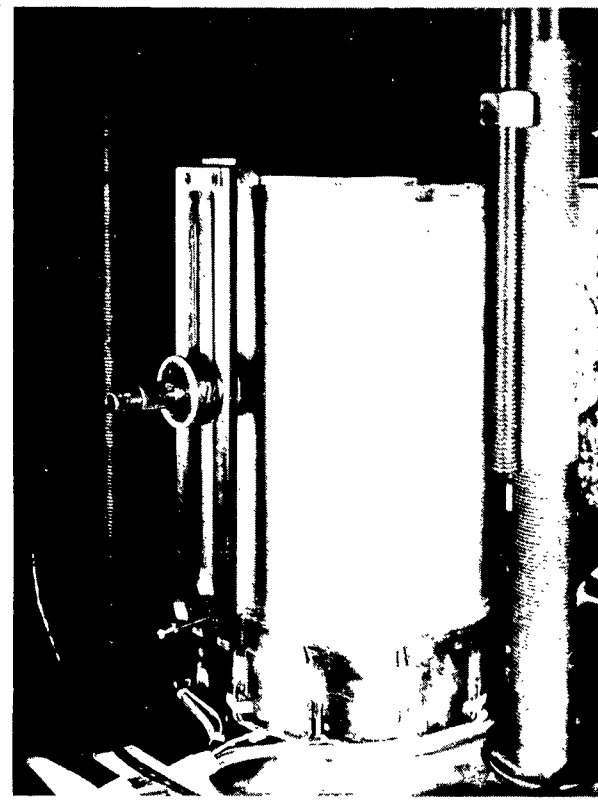

Fig. 2. Set up for Initial Imperfection Measurements. Photograph courtesy of C. D. Babcock, Jr.

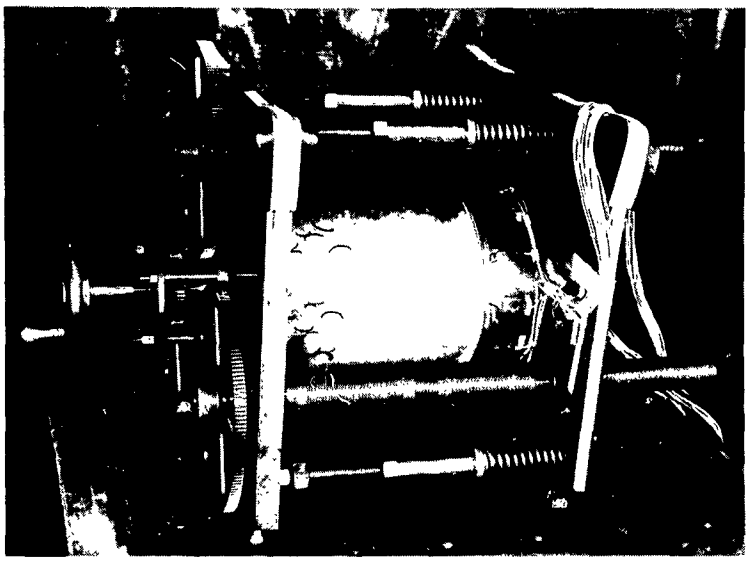

Fig. 3. Testing Machine with Shell in Testing Position. Photograph courtesy of C. D. Babcock, Jr.

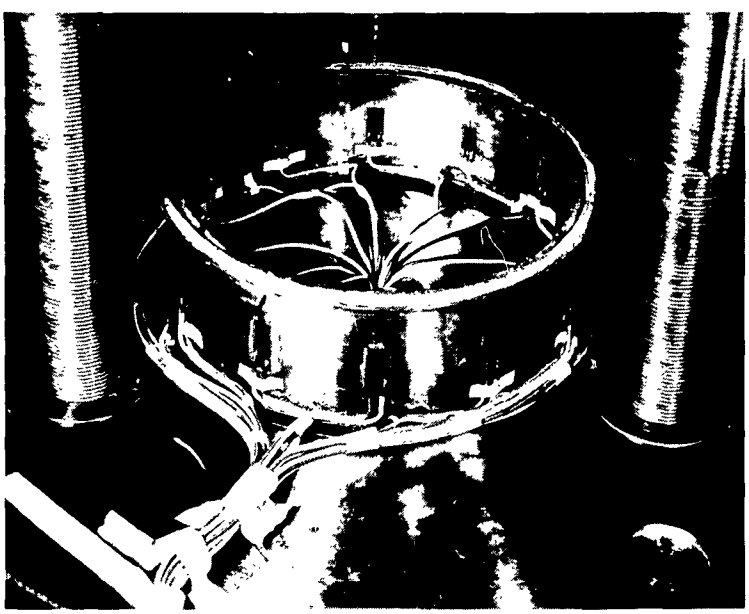

Fig. 4. Load Measuring Ring. Photograph courtesy of C. D. Babcock, Jr.

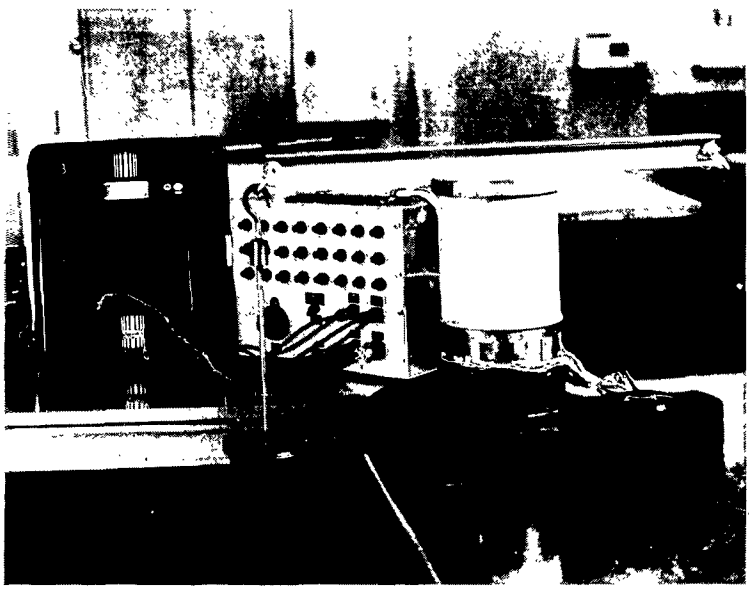

Fig. 5. Test Set up for Load Ring Calibration in Bending.

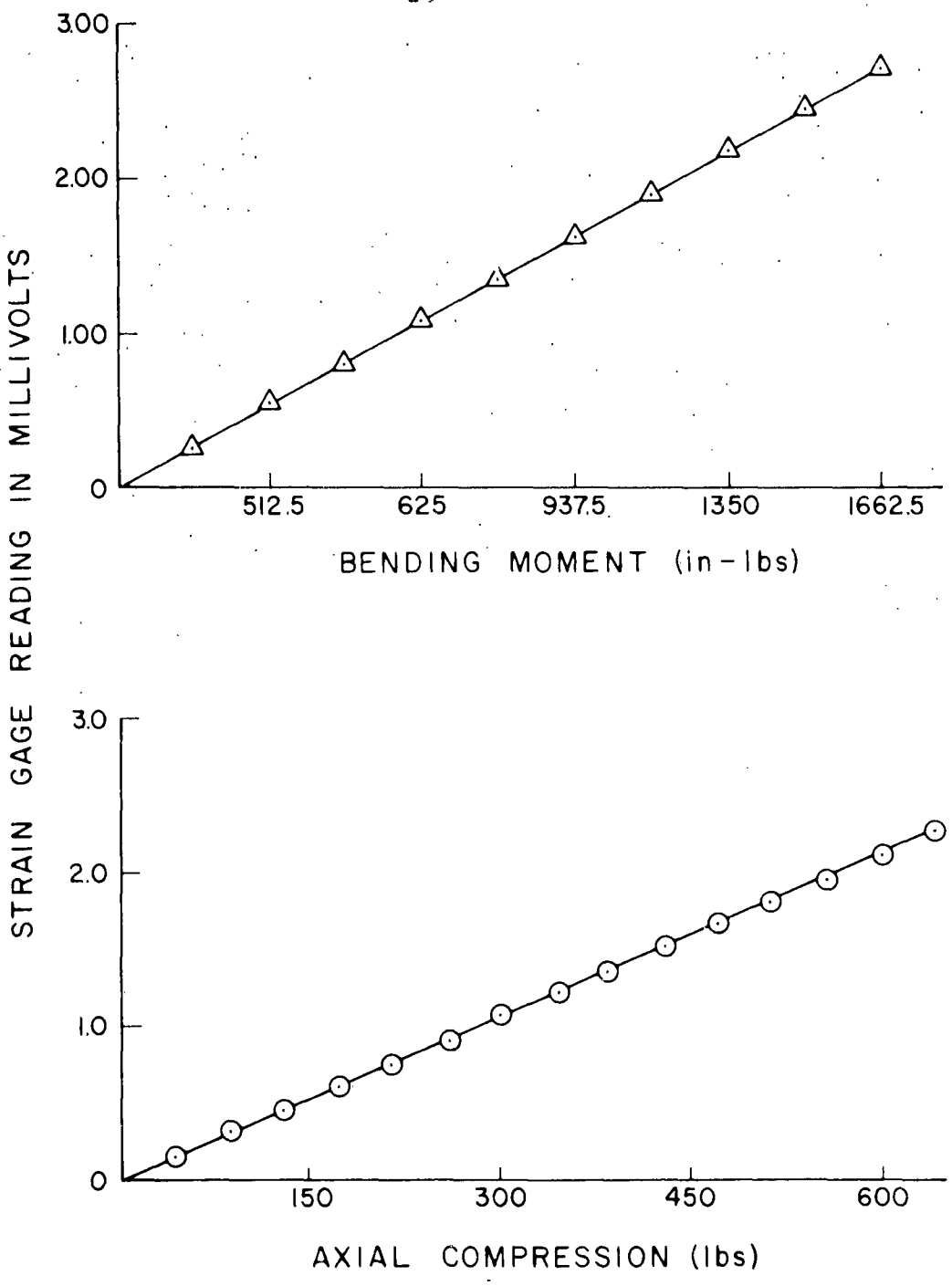

Fig. 6. Load Ring Calibration Results.

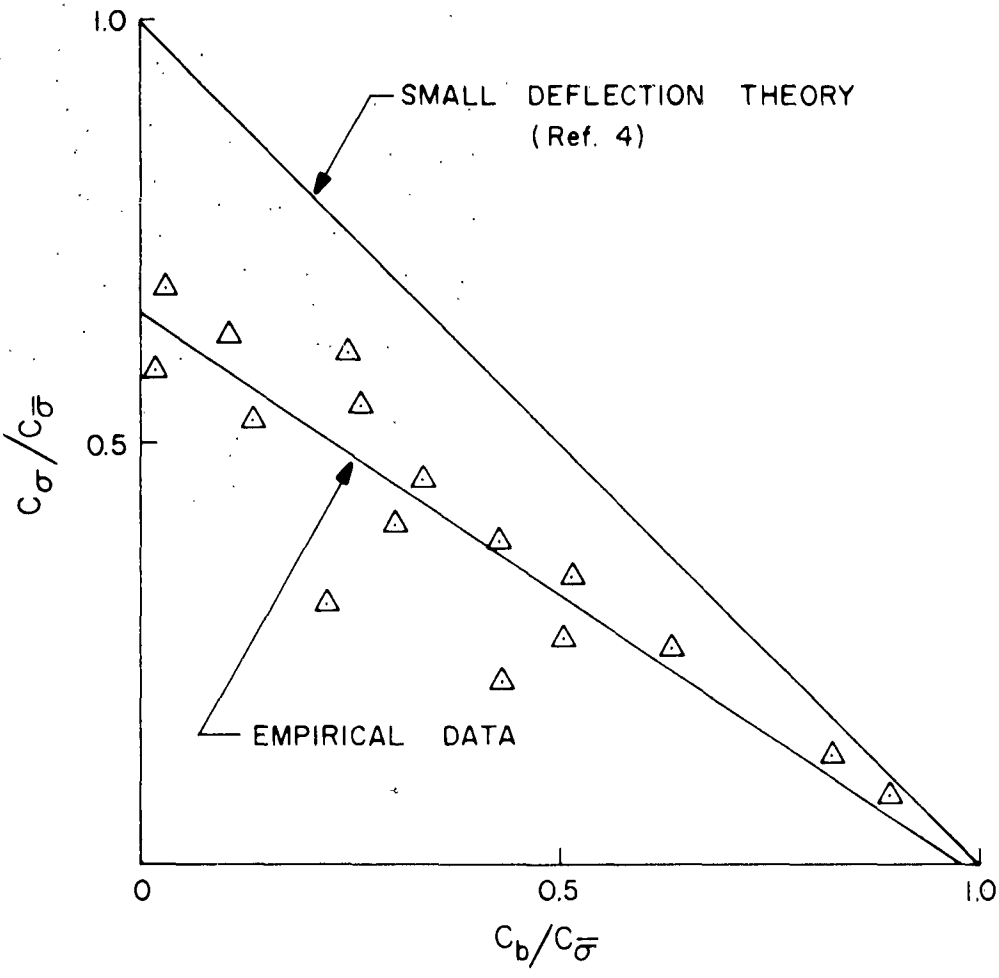

Fig. 7. Interaction Curve, Axial Compression and Bending.

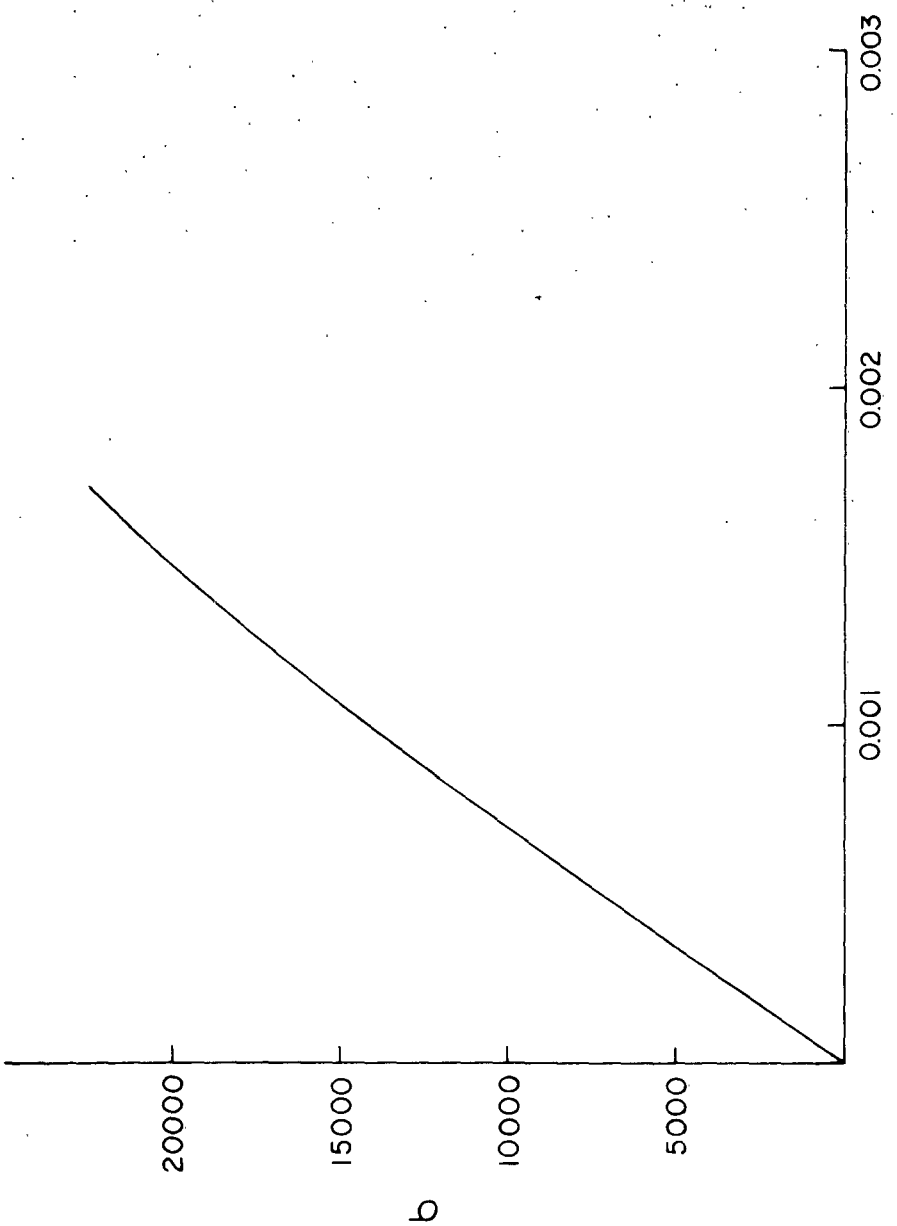

Fig. 8. Typical Stress Strain Curve for Plated Copper.

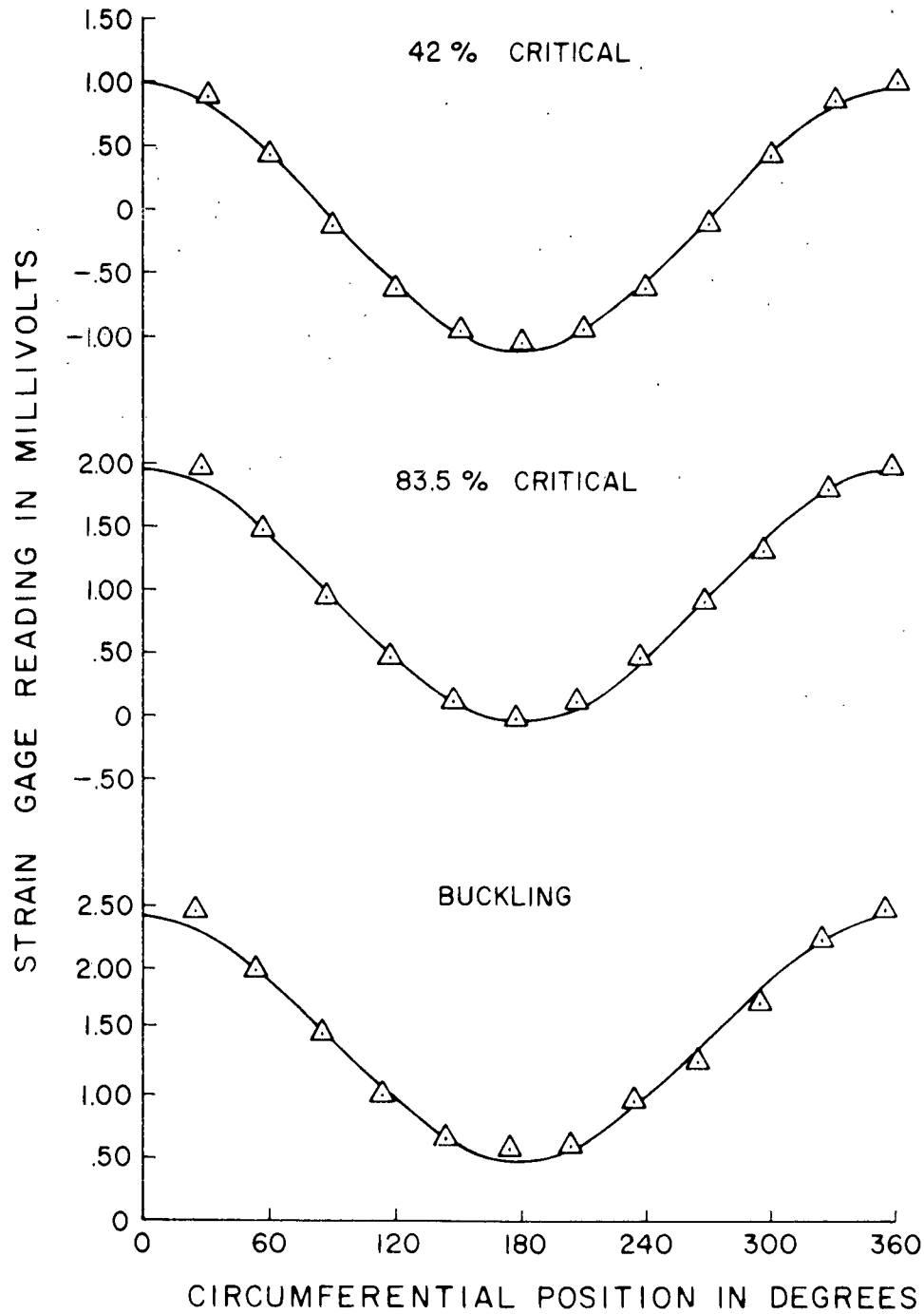

Fig. 9. Comparison of Computed Load Distribution with Strain Gage Data for Various Increments of Loading; Shell S-1.

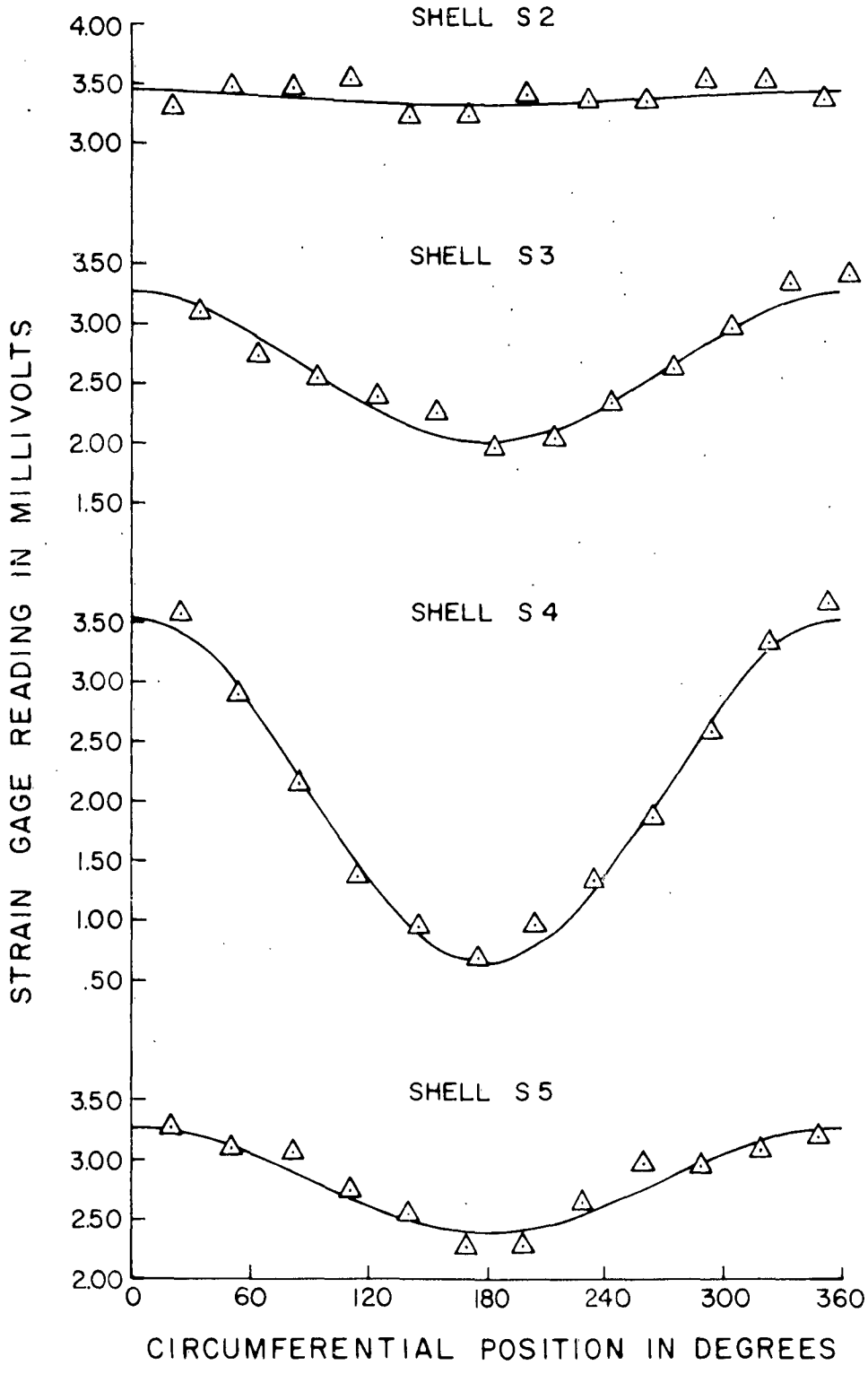

Fig. 10. Comparison of Computed Load Distribution with Strain Gage Data at Buckling, Shells S2, S3, S4, and S5.

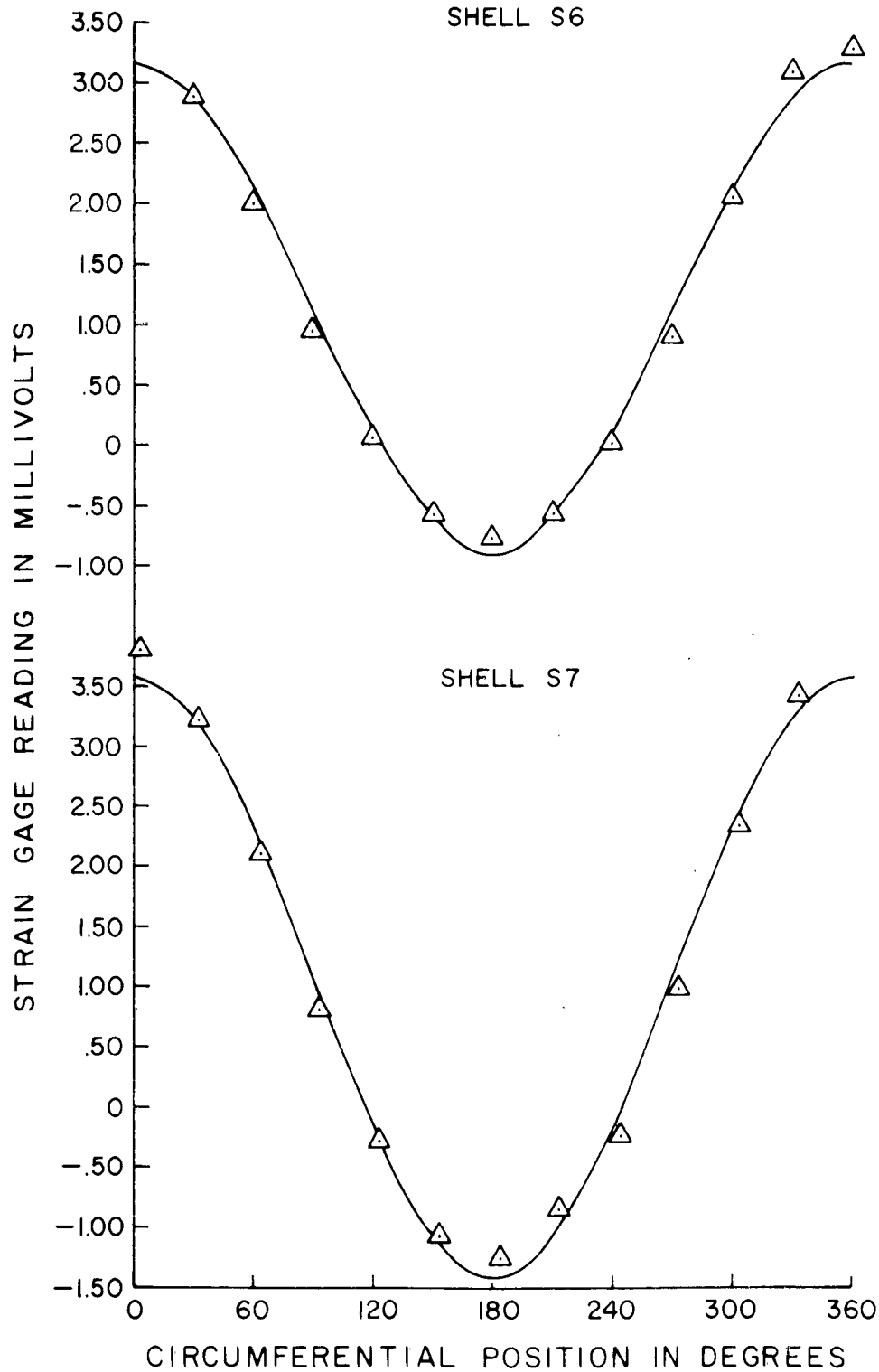

Fig. 11. Comparison of Computed Load Distribution with Strain Gage Data at Buckling, Shells S6 and S7.

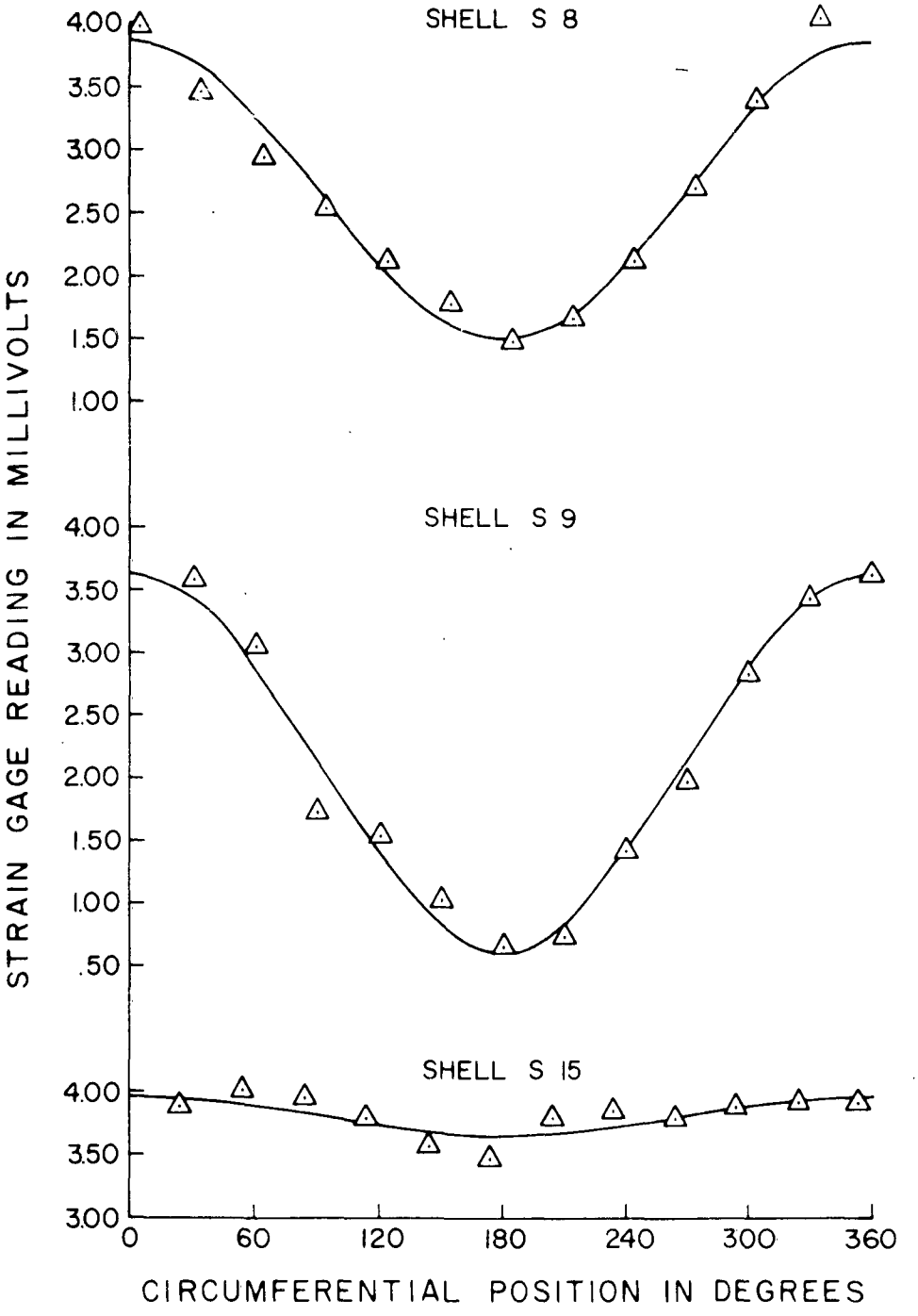

Fig. 12. Comparison of Computed Load Distribution with Strain Gage Data at Buckling, Shells S8, S9, and S15.

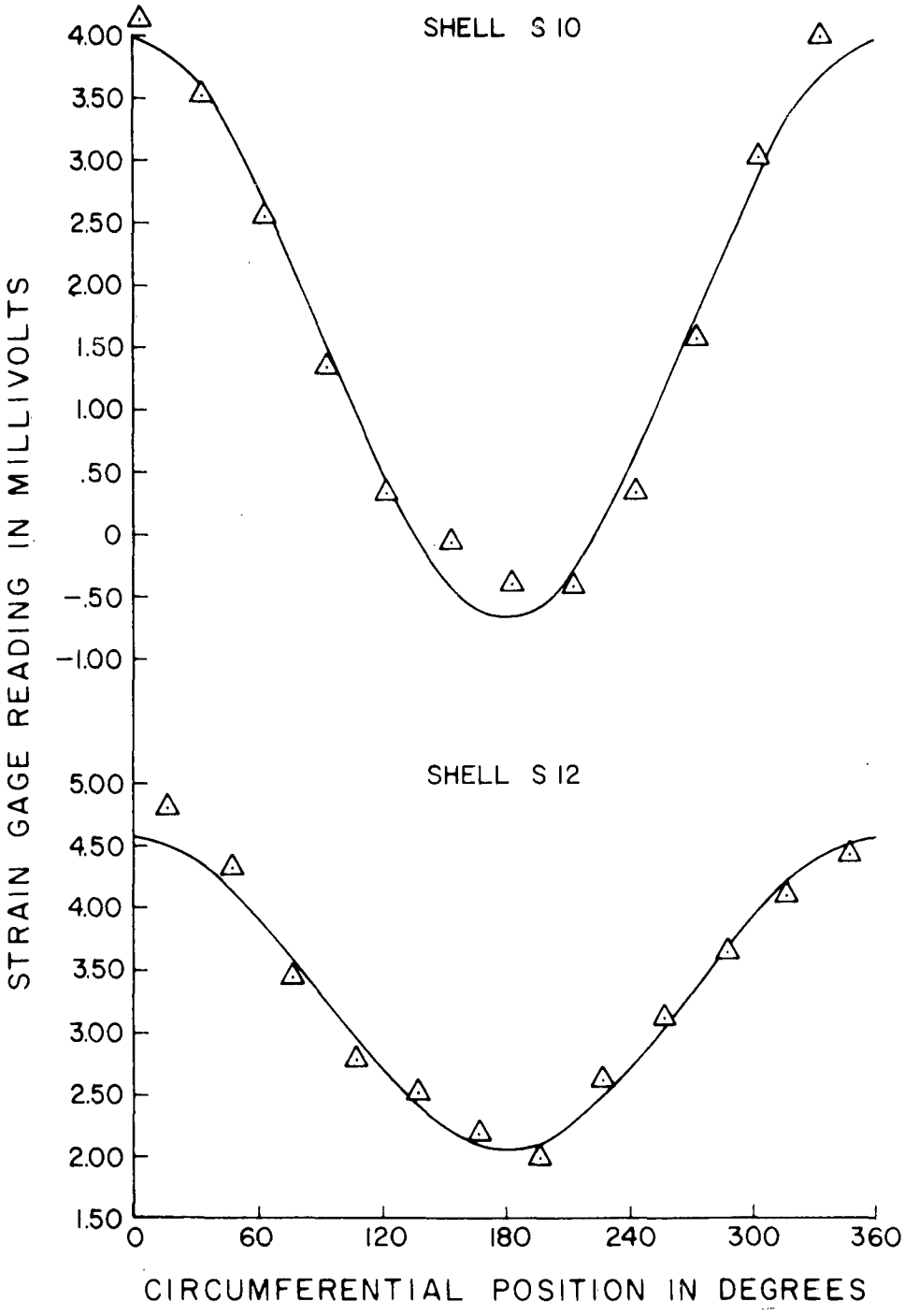

Fig. 13. Comparison of Computed Load Distribution with Strain Gage Data at Buckling, Shells, S10, and S12.

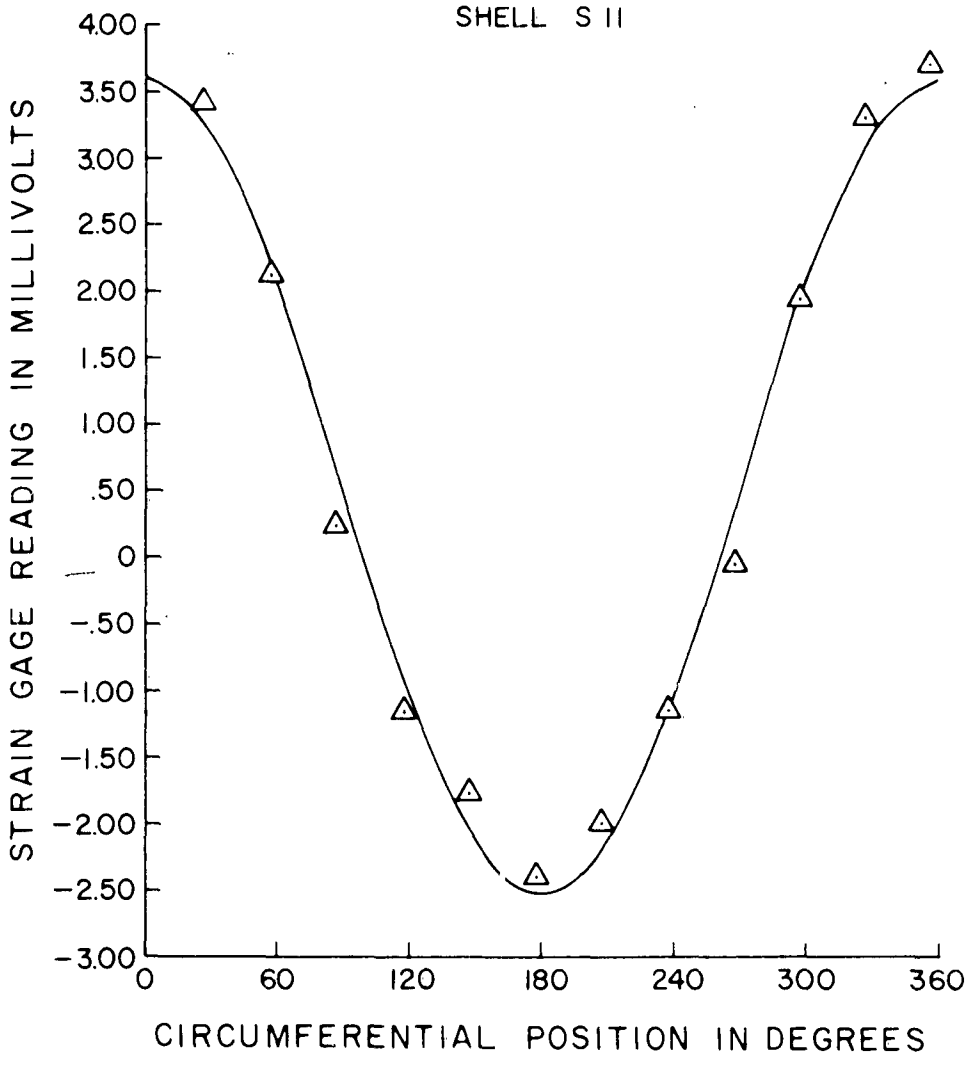

Fig. 14. Comparison of Computer Load Distribution with Strain Gage Data at Buckling, Shell, S11.

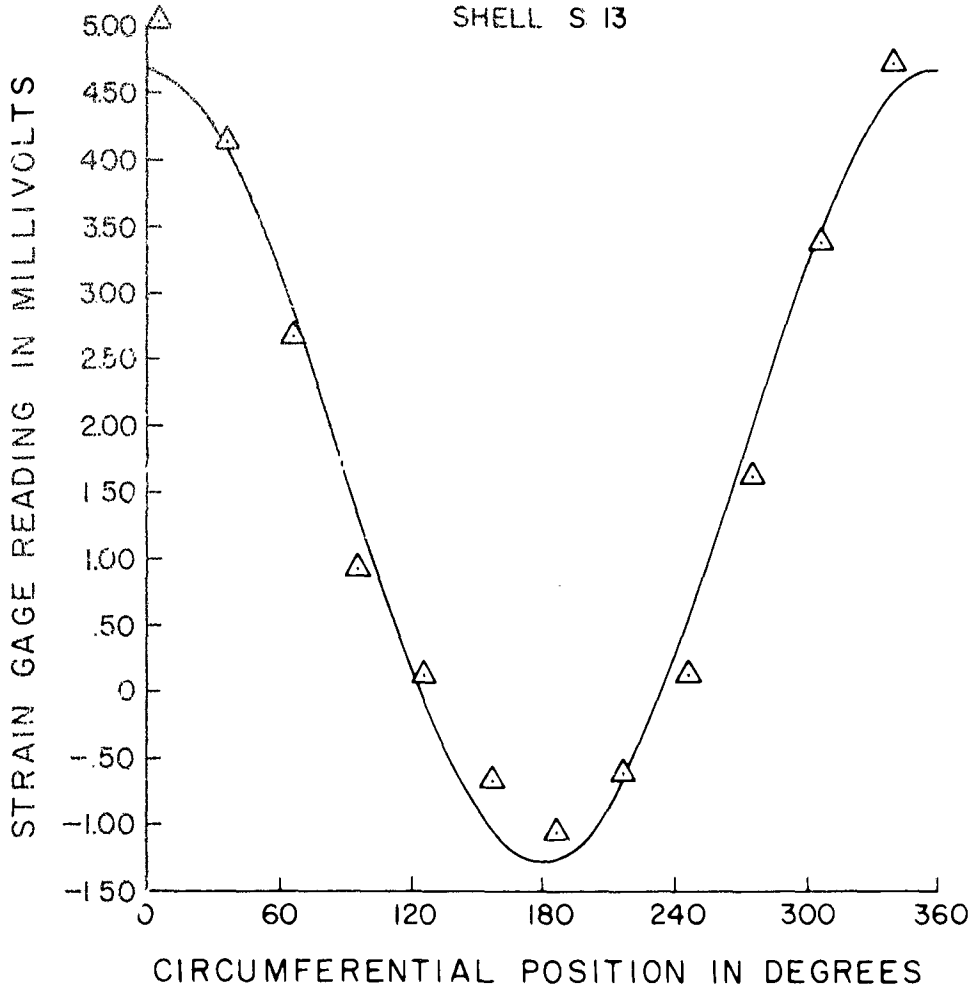

Fig. 15. Comparison of Computer Load Distribution with Strain Gage Data at Buckling, Shell, S13.

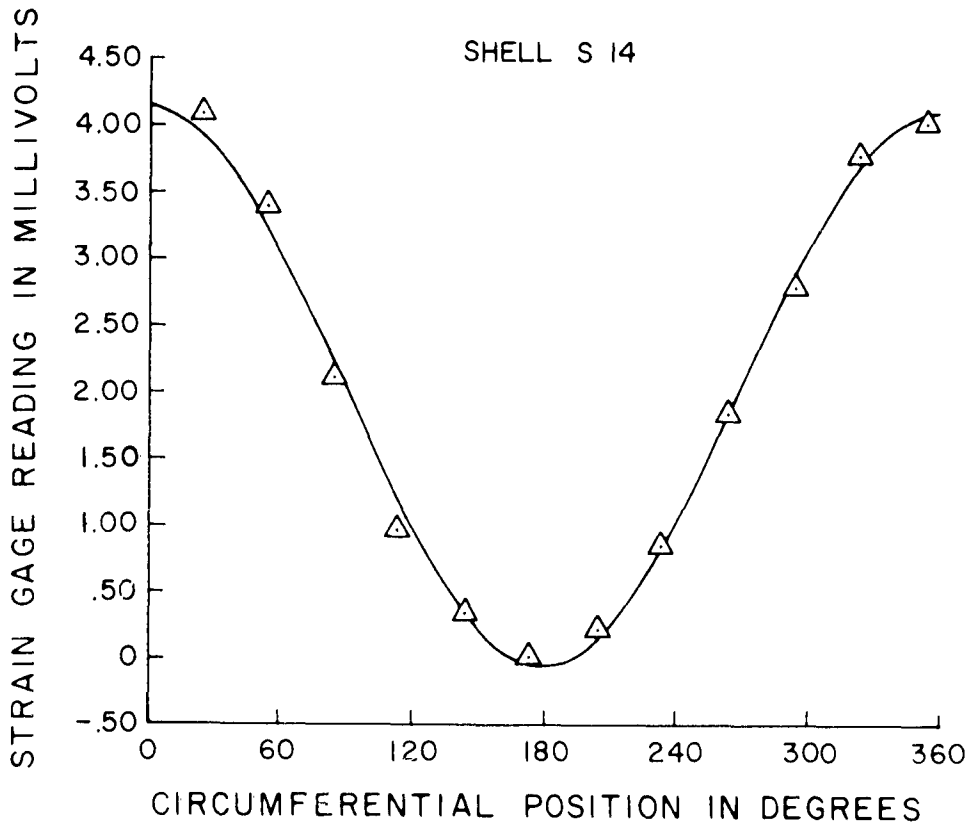

Fig. 16. Comparison of Computer Load Distribution with Strain Gage Data at Buckling, Shell S14.

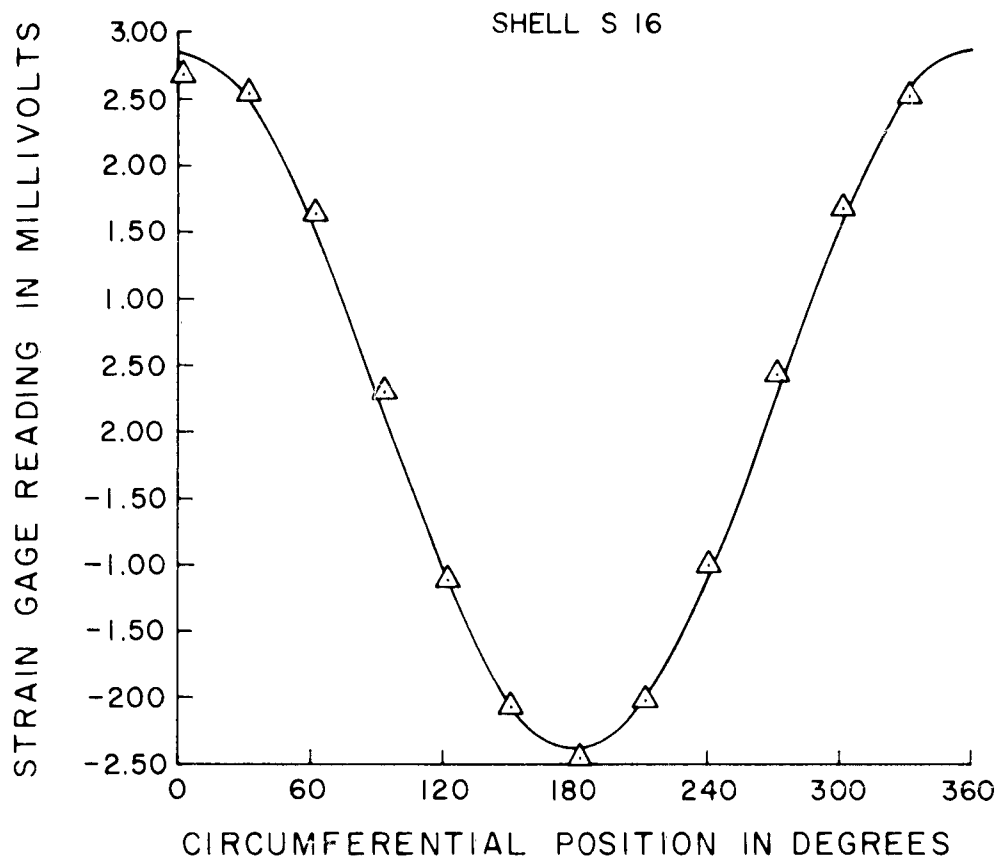

Fig. 17. Comparison of Computer Load Distribution with Strain Gage Data at Buckling, Shell S1é.

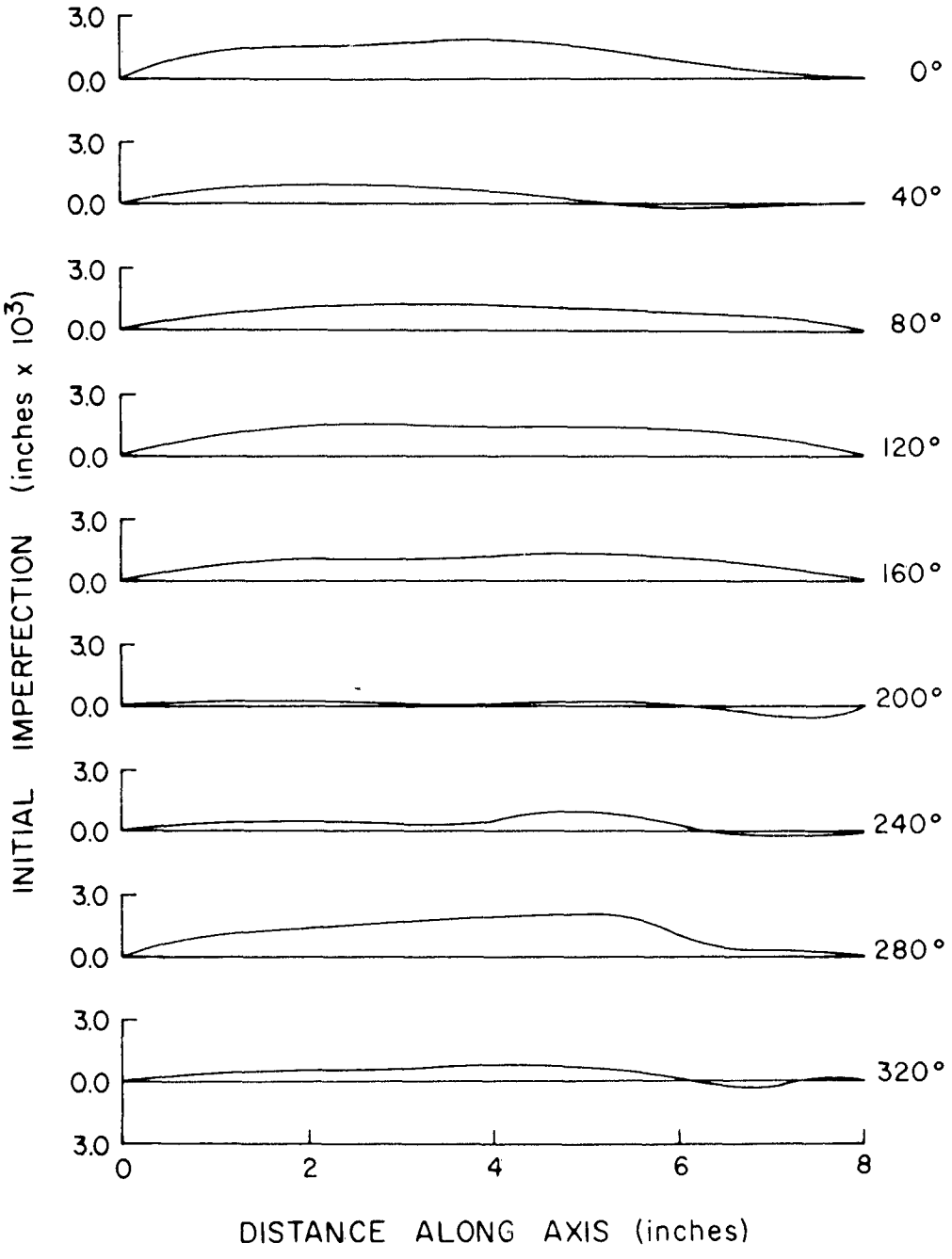

Fig. 18. Initial Imperfection, Shell S1.

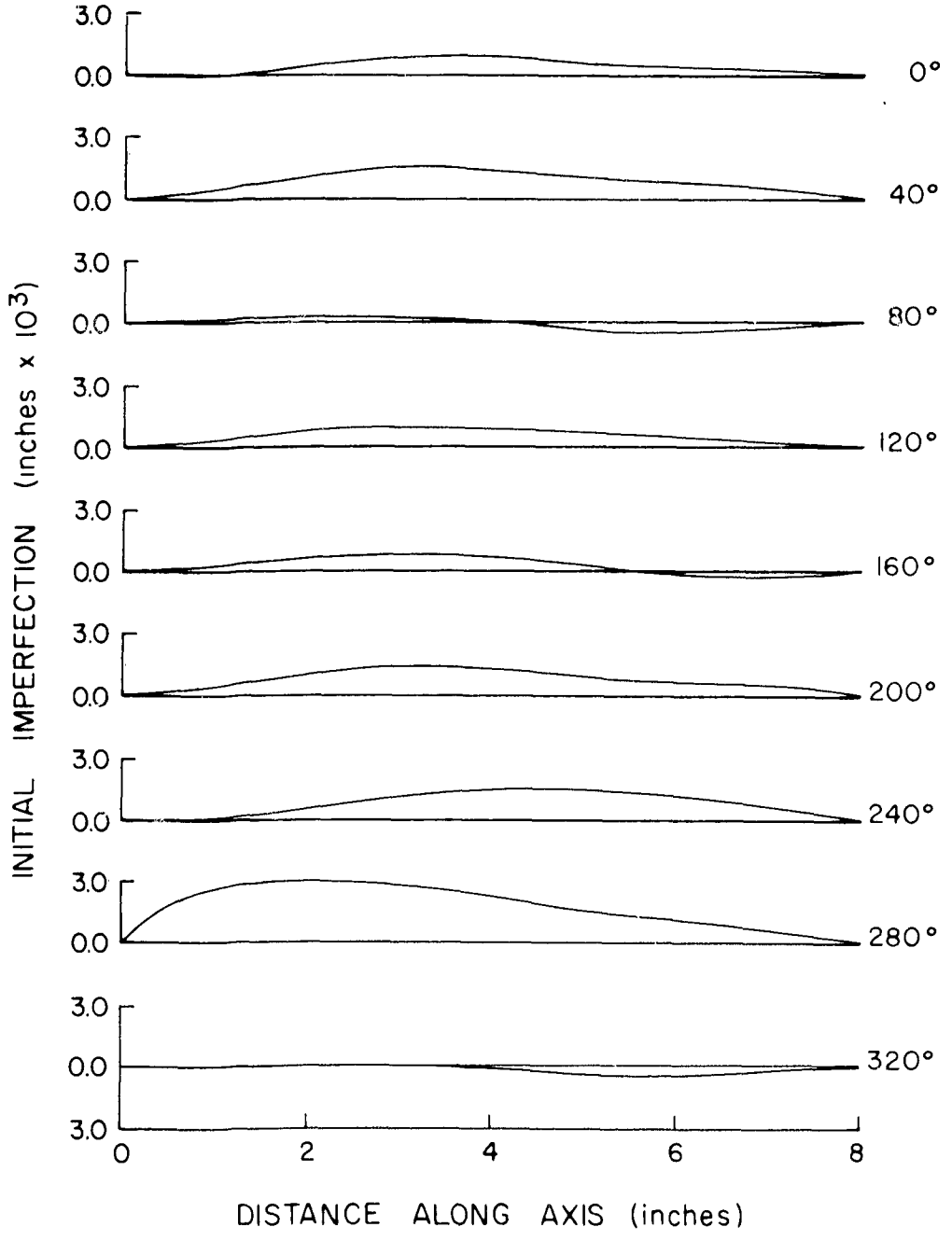

Fig. 19. Initial Imperfection, Shell S4.

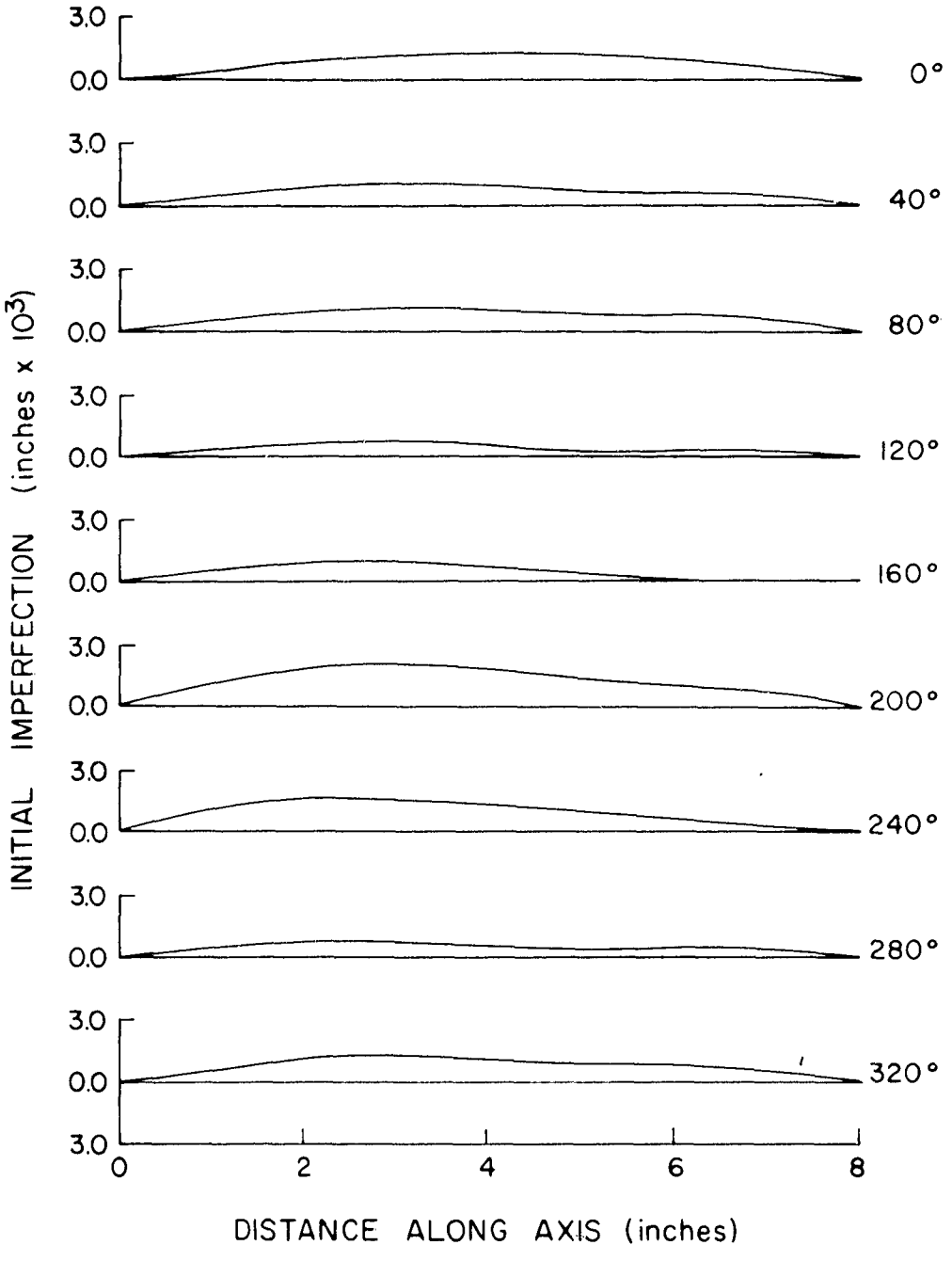

Fig. 20. Initial Imperfection, Shell S8.